The final publication is available at Elsevier via https://doi.org/10.1016/j.ijimpeng.2018.12.004 © 2018. This manuscript version is made available under the CC-BY-NC-ND 4.0 license http://creativecommons.org/licenses/by-nc-nd/4.0/

Accepted Manuscript

Simulations for three-dimensional landmine detonation using the SPH method

Jian-Yu Chen, Chong Peng, Fue-Sang Lien

PII: S0734-743X(18)30920-5
DOI: https://doi.org/10.1016/j.ijimpeng.2018.12.004
Reference: IE 3214

To appear in: *International Journal of Impact Engineering*

Received date: 15 September 2018
Revised date: 10 December 2018
Accepted date: 10 December 2018

Please cite this article as: Jian-Yu Chen, Chong Peng, Fue-Sang Lien, Simulations for three-dimensional landmine detonation using the SPH method, *International Journal of Impact Engineering* (2018), doi: https://doi.org/10.1016/j.ijimpeng.2018.12.004

This is a PDF file of an unedited manuscript that has been accepted for publication. As a service to our customers we are providing this early version of the manuscript. The manuscript will undergo copyediting, typesetting, and review of the resulting proof before it is published in its final form. Please note that during the production process errors may be discovered which could affect the content, and all legal disclaimers that apply to the journal pertain.

ACCEPTED MANUSCRIPT

Highlights

- The modified SPH method in combination with the elastoplastic and hypoplastic constitutive models is employed to tackle the large deformation in 3D landmine detonations for the first time.
- The modified continuity equation is applied to tackle multiphase interfaces with a high density ratio in soil explosion.
- The accuracy of the SPH method is improved by using the Kernel Gradient Correction (KGC) technique.
- The Open-MP programming interface is incorporated for the parallelization and computational efficiency of the in-house SPH code.
- A wide range of validations are conducted against both fairly new experimental data and other numerical results.

ACCEPTED MANUSCRIPT

ACCEPTED MANUSCRIPT

Simulations for three-dimensional landmine detonation using the SPH method

Jian-Yu Chen[a,*], Chong Peng[b,c], Fue-Sang Lien[a]

[a]*Department of Mechanical and Mechatronics Engineering, University of Waterloo, 200 University Avenue West, Waterloo, Ontario, N2L 3G1, CANADA.*
[b]*ESS Engineering Software Steyr GmbH, Berggasse 35, 4400 Steyr, Austria*
[c]*Institut für Geotechnik, Universität für Bodenkultur, Feistmantelstrasse 4, 1180 Vienna, Austria*

Abstract

The simulation of the soil fragmentation under buried explosive detonation is an extremely difficult task. In this paper, the modified smoothed particle hydrodynamics method (SPH) in combination with the elastoplastic and hypoplastic constitutive models is introduced to simulate the three-dimensional (3D) landmine detonation for the first time. The modified continuity equation is incorporated to tackle the multiphase interfacial problems with high density ratios. The elastoplastic and hypoplastic constitutive models are employed to describe the soil mechanical behavior. Furthermore, the in-house SPH code is parallelized using the Open-MP program interface to solve problems with large number of particles efficiently. At the end, the simulation results are compared with the experimental data, which shows that the SPH method in conjunction with these two constitutive models can tackle landmine detonation problems involving large deformation very well.

Keywords: Smoothed particle hydrodynamics, Multiphase interface, Landmine detonation, Elastoplastic, Hypoplastic, Open-MP

1. Introduction

Shallow-buried explosives detonations are common threats in conflict areas all over the world. The blast loading and soil throw can cause significant damage on human body such as spinal cord compression and brain damage. In order to understand physical process of landmine detonation, numerous soil explosion experiments have been conducted. Bergeron et al. conducted the detonation of 100-gram charge of C4 explosive to study the basic explosion physics of shallow-buried charges and to generate a high-quality data set for the validation of computer codes [1]. Rigby et al. developed soil explosion apparatus and measured spatial pressure distribution from explosives buried in dry sand [2, 3]. However, in comparison with the numerical methods, the experiments have limited use in treating complex problems due to its configuration costs, scaling difficulties, and measurement issues.

The simulations of dynamic behaviors of soil under explosive detonation have attracted much attention in recent years, as it can provide a numerical tool for engineering problems such as military vehicles design and disaster mitigation. Conventional methods, such as the finite element method (FEM), the finite difference method (FDM), and the finite volume method (FVM), have been widely applied in computational geodynamics. However, within the framework of these conventional methods, the problems involving extremely large deformation can cause severe mesh distortion, and even program abort. In addition, the meshing and re-meshing in the solution domain are always difficult and time-consuming especially for the problems with complex geometries.

In the last three decades, numerous mesh-free particle methods and their modified versions, such as the smoothed particle hydrodynamics (SPH) method, the peridynamics method and the discrete element method (DEM), have been proposed to deal with the problems with large deformation. In comparison with the conventional methods, these mesh-free

*Corresponding author
Email addresses: j492chen@uwaterloo.ca (Jian-Yu Chen), pengchong07@gmail.com (Chong Peng), fue-sang.lien@uwaterloo.ca (Fue-Sang Lien)

ACCEPTED MANUSCRIPT

methods require no mesh in computation, and thus they can tackle large deformation problems like high velocity impact and crack propagation. For example, Rabczuk et al. proposed a simplified cracking mesh-free particle method (CPM) for arbitrary involving cracks, and the numerical results show that the CPM method can replicate crack paths and handle crack branching and fragmentation [4, 5, 6, 7, 8]. Rabczuk et al. also presented immersed particle method for fluid-structure interaction and a dual-horizon peridynamics method (DP-PD) for modeling dynamic fractures [9, 10, 11]. In this paper, the SPH method is employed to simulate the soil explosion problems. SPH is a well established lagrangian method proposed by Managhan and Lucy [12, 13], and it has wide applications in astrophysics and computational fluid dynamics (CFD) such as the detonation and high velocity impact problems. The principal concept of the SPH method is the use of statistical techniques to replace analytical formulations for the physical properties with a distribution of fluid elements. Hedayati et al. conducted the modeling and simulation of the penetration of steel on ceramic/aluminum target using SPH [14]. Rabczuk et al. investigated the fragmentation of concrete due to explosive loading, which suggests that the SPH method can predict the damage of the concrete slabs [15, 16, 17]. A variety of simulations for air and underwater explosions and their damage to steel and reinforced concrete slabs using the SPH method have also been reported in [18, 19, 20, 21].

In order to apply the SPH method to simulate landmine detonation problems, an appropriate soil constitutive model is essential. Bui et al. implemented the elastoplastic constitutive model in conjunction with the Drucker-Prager yield criterion into SPH to study the elastic and plastic behaviors of soil [22, 23]. Peng et al. employed the hypoplastic constitutive model to simulate geomechanics problems within the framework of SPH, which shows a good performance compared to analytical and experimental results [24, 25]. Fan and Li combined the peridynamics and the SPH methods and implemented three types of soil constitutive models to investigate the blast fragmentation of soil under buried explosives [26, 27, 28, 29, 30]. Although numerous studies have been conducted in the area of geomechanics, the research of 3D landmine detonation simulation is still in its infancy. Our research group has developed an in-house SPH code to investigate 2D soil explosion and its effects on structures, and a general agreement between our SPH predictions and the experimental data was observed [31]. However, the 2D model is still of limited use for engineering applications. Thus, in our current work compared to the previous research in two dimensions, another new soil constitutive model - the hypoplastic model which can capture some salient behaviors of soils is implemented, and the 3D soil explosion modelling using the Open-MP programming interface is established further. In comparison with the previous studies on soil fragmentation simulations, the modified SPH method in conjunction with the elastoplastic and hypoplastic constitutive models are employed to tackle the 3D landmine detonation for the first time.

This paper is organized into six sections. In Section 2, the fundamentals of the SPH method, artificial viscosity, boundary conditions, and kernel gradient correction are brifely introduced. In Section 3, the elastoplastic model and hypoplastic model are described in detail. In Section 4, some benchmark cases are tested to validate the explosion model and these two soil constitutive models. In Section 5, the 3D soil explosion is simulated, and the simulation results of the elastoplastic and the hypoplastic constitutive models are compared with the experimental data from [3].

2. Fundamentals of the SPH method

2.1. Function approximation in SPH

The SPH method can be divided into two parts: kernel approximation and particle approximation. In the kernel approximation, the function $f(\boldsymbol{x})$ and the function derivative $\nabla f(\boldsymbol{x})$ are approximated by

$$\langle f(\boldsymbol{x})\rangle = \int_{\Omega} f(\boldsymbol{x}')W(\boldsymbol{x}-\boldsymbol{x}',h)d\boldsymbol{x}' \tag{1}$$

$$\langle \nabla f(\boldsymbol{x}) \rangle = -\int_{\Omega} f(\boldsymbol{x}') \nabla W(\boldsymbol{x} - \boldsymbol{x}', h) d\boldsymbol{x}' \tag{2}$$

where f is a function of vector $\boldsymbol{x}$, W is the kernel function, and h is the smoothing length. The cubic spline kernel function below is applied in this work.

$$W(q,h) = \alpha_d \begin{cases} \frac{2}{3} - q^2 + \frac{1}{2}q^3 & 0 \le q < 1 \\ \frac{1}{6}(2-q)^3 & 1 \le q < 2 \\ 0 & q \ge 2 \end{cases} \tag{3}$$

in which q is the normalized distance between two particles and defined as $q = r/h$, and r is the Euclidean distance. α_d is a normalization factor, and the value is $15/(7\pi h^2)$ in two dimensions and $3/(2\pi h^3)$ in three dimensions. The smoothing length h of particle i in the landmine detonation is updated using the following equation,

$$\frac{dh_i}{dt} = -\frac{1}{d}\frac{h_i}{\rho_i}\frac{d\rho_i}{dt} \tag{4}$$

in which d is the dimension of a given problem, and ρ_i is the density of particle i. The second step of the SPH derivation is the particle approximation. The physical values of particle i can be approximated by the summation of particles in the support domain of particle i (see Fig. 1). The particles approximation of function derivative $\nabla f(\boldsymbol{x})$ can be obtained in the same manner,

$$\langle f(\boldsymbol{x}_i) \rangle = \sum_{j=1}^{N} f(\boldsymbol{x}_j) W_{ij} \frac{m_j}{\rho_j} \tag{5}$$

$$\langle \nabla f(\boldsymbol{x}_i) \rangle = -\sum_{j=1}^{N} f(\boldsymbol{x}_j) \nabla W_{ij} \frac{m_j}{\rho_j} \tag{6}$$

in which, ρ_i, m_i are density and mass of particle i, respectively.

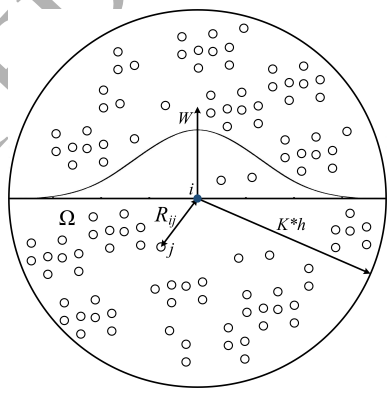

Figure 1: Particles approximation of the SPH method in a 2D problem; Ω is the support domain of particle i; $K * h$ is the range of the support domain; R_{ij} is the distance between two particles.

2.2. Discretized equations for Navier-Stokes (N-S) equation

As we know, a second-order stress tensor consists of a spherical part and a deviatoric part:

$$\sigma^{\alpha\beta} = -p\delta^{\alpha\beta} + S^{\alpha\beta} \tag{7}$$

ACCEPTED MANUSCRIPT

in which $-p\delta^{\alpha\beta}$ is the hydrostatic stress and $S^{\alpha\beta}$ is the deviatoric stress. With the basics of the SPH method mentioned above, the governing equations can be discretized in the following.

$$\begin{cases} \frac{\mathrm{d}\rho_i}{\mathrm{d}t} = \sum_{j=1}^{N} m_j v_{ij}^{\alpha} \cdot \frac{\partial W_{ij}}{\partial x_i^{\alpha}} & (a) \\ \frac{\mathrm{d}v_i^{\alpha}}{\mathrm{d}t} = \sum_{j=1}^{N} m_j \frac{\sigma_i^{\alpha\beta} + \sigma_j^{\alpha\beta}}{\rho_i \rho_j} \frac{\partial W_{ij}}{\partial x_i^{\beta}} & (b) \\ \frac{\mathrm{d}e_i}{\mathrm{d}t} = \frac{1}{2} \sum_{j=1}^{N} m_j \frac{p_i + p_j}{\rho_i \rho_j} v_{ij}^{\beta} \cdot \frac{\partial W_{ij}}{\partial x_i^{\beta}} + \frac{1}{2\rho_i} S_i^{\alpha\beta} \varepsilon_i^{\alpha\beta} & (c) \\ p_i = p(\rho_i, e_i) & (d) \end{cases} \tag{8}$$

where ρ_i, v_i, e_i, p_i, m_i are density, velocity, internal energy, pressure, and mass of particle i; $\frac{\mathrm{d}()}{\mathrm{d}t}$ is the time derivative of physical quantities; $v_{ij}^{\alpha} = v_i^{\alpha} - v_j^{\alpha}$. Equation (8 (d)) can be elaborated further in the following. For the detonation simulations with C4 explosive charge, the Jones-Wilkins-Lee (JWL) equation of state (EOS) is used and defined as,

$$p = A(1 - \frac{w\eta}{R_1})e^{-\frac{R_1}{\eta}} + B(1 - \frac{w\eta}{R_2})e^{-\frac{R_2}{\eta}} + w\eta\rho_0 E \tag{9}$$

where η is the ratio of the detonation products density to the initial density of the explosive; A, B, R_1, R_2, w are fitting coefficients; ρ_0 is the initial density; E is the specific internal energy per unit mass.

In the soil modelling and simulations, the hydrostatic pressure p is calculated directly from the soil constitutive equation by the definition of mean stress, rather than from an equation of state (EOS):

$$p = -\frac{\sigma^{\alpha\alpha}}{3} = -\frac{1}{3}(\sigma^{11} + \sigma^{22} + \sigma^{33}) \tag{10}$$

where σ^{11}, σ^{22}, σ^{33} are the components of the normal stress tensor in x, y and z directions, respectively.

2.3. Interface treatment

The interface treatment of landmine detonation is a complex issue in the SPH method. The physical variables of the particles near the multiphase interface are obtained by the summation of the neighbouring particles from both soil and explosive gas, and the density ratio between the soil and the expanded explosive gas is very large (see Fig. 2), which may generate inaccurate and unphysical values during the computation. In order to get stable and accurate numerical results for detonation problems with high density ratios, the mass conservation equation should be modified as [32],

$$\frac{\mathrm{d}\rho_i}{\mathrm{d}t} = \sum_{j=1}^{N} \frac{\rho_i + \psi_i \rho_j}{(1 + \psi_i)\rho_j} m_j v_{ij}^{\alpha} \cdot \frac{\partial W_{ij}}{\partial x_i^{\alpha}} \tag{11}$$

in which,

$$\psi_i = \frac{1}{lnk_i} \tag{12}$$

$$k_i = \frac{\rho_{i,max}}{\rho_{i,min}} \tag{13}$$

where $\rho_{i,min}$ and $\rho_{i,max}$ are the particles with minimum and maximum densities in the support domain of particle i, respectively. For more derivation details about this modified continuity equation, please refer to [32].

ACCEPTED MANUSCRIPT

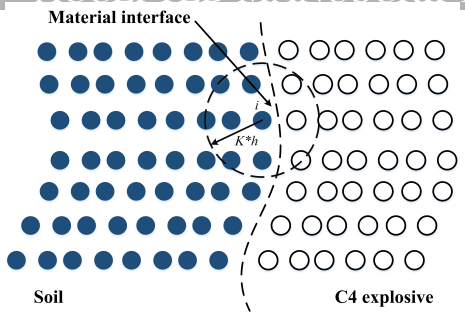

Figure 2: Soil and C4 explosive particles near the interface.

2.4. Artificial viscosity

To alleviate unphysical oscillations and stabilize the numerical scheme, the Monaghan type artificial viscosity is incorporated into the momentum equation in the following way [33].

$$\Pi_{ij} = \begin{cases} \frac{-\alpha c_{ij}\phi_{ij} + \beta\phi_{ij}^2}{\rho_{ij}} & \boldsymbol{v}_{ij}\cdot\boldsymbol{x}_{ij} < 0 \\ 0 & \boldsymbol{v}_{ij}\cdot\boldsymbol{x}_{ij} \geq 0 \end{cases} \tag{14}$$

$\phi_{ij} = \frac{h_{ij}\boldsymbol{v}_{ij}\cdot\boldsymbol{x}_{ij}}{|\boldsymbol{x}_{ij}|^2+(\varphi)^2}$, $c_{ij} = \frac{1}{2}(c_i + c_j)$, $\rho_{ij} = \frac{1}{2}(\rho_i + \rho_j)$, $h_{ij} = \frac{1}{2}(h_i + h_j)$, $\boldsymbol{v}_{ij} = \boldsymbol{v_i} - \boldsymbol{v_j}$, $\boldsymbol{x}_{ij} = \boldsymbol{x}_i - \boldsymbol{x}_j$,

where c_i is the sound speed of particle i; α and β are constant coefficients that are set around 1.0 and 10.0 for the detonation problems, respectively; $\varphi = 0.1h_{ij}$ is applied to prevent the numerical divergence when two particles approach each other. Thus the momentum equation should be modified as,

$$\frac{\mathrm{d}v_i^\alpha}{\mathrm{d}t} = \sum_{j=1}^{N} m_j\left(\frac{\sigma_i^{\alpha\beta} + \sigma_j^{\alpha\beta}}{\rho_i\rho_j} + \Pi_{ij}\delta^{\alpha\beta}\right)\frac{\partial W_{ij}}{\partial x_i^\beta} \tag{15}$$

2.5. Boundary conditions

Boundary treatment is one of the particularly important issues in the SPH method. The SPH method may suffer from the particle deficiency near or on the boundary. Different methods have been proposed in the past to tackle this problem [34, 35, 36]. In this paper, several layers of dummy particles are used to represent the solid wall [37] (see Fig. 3). This boundary implementation method is suitable for sharp corners and complex geometries. The velocity of dummy particle is set to either zero or the velocity of solid wall, which represents the fixed boundary and moving boundary conditions, respectively. For a real paticle i, the stress tensor of dummy particle j is assigned to the same value as particle i, i.e. $\sigma_i^{\alpha\beta} = \sigma_j^{\alpha\beta}$, if particle j is a neighbor of the particle i.

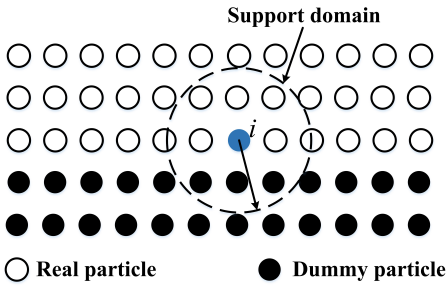

Figure 3: Sketch of solid boundary treatment: dummy particles for a nonslip boundary.

ACCEPTED MANUSCRIPT

2.6. Explicit time integration

Equations (8 (a)), (8 (b)), and (8 (c)) are integrated using the standard Leapfrog method to update the density ρ, velocity v, and energy e:

$$\rho_{n+1/2} = \rho_{n-1/2} + \Delta t \left(\frac{d\rho}{dt}\right)_n \tag{16}$$

$$v^{\alpha}_{n+1/2} = v^{\alpha}_{n-1/2} + \Delta t \left(\frac{dv^{\alpha}}{dt}\right)_n \tag{17}$$

$$e_{n+1/2} = e_{n-1/2} + \Delta t \left(\frac{de}{dt}\right)_n \tag{18}$$

$$x^{\alpha}_{n+1} = x^{\alpha}_{n} + \Delta t v^{\alpha}_{n+1/2} \tag{19}$$

where x is the coordinate of particles; Δt is the time step; n denotes the current calculation step.
In addition, the CFL (Courant-Friedichs-Levy) condition, governing the stability of the Leapfrog method, should be satisfied by the following time step:

$$\Delta t \leq 0.2(h/c) \tag{20}$$

in which c is the sound speed of soil. In this paper, the sound speed is calculated by $c = \sqrt{E/\rho}$, where E is the Young's modulus and ρ is the density of the soil, respectively.

2.7. The correction of kernel gradient

The second order accuracy of the interior region is ensured by the continuous kernel interpolation of equation (1). However, this C^1 consistency is not always satisfied due to the irrigular distributions of particles and the deficiency near the boundary, which may lead to relatively low accuracy of the conventional SPH method. A variety of corrective procedures have been proposed to improve the particle inconsistency and accuracy of the kernel-based approximations [25, 38, 39]. In this paper, the kernel gradient correction [40] is applied to enforce C^1 consistency, and is given as follows,

$$\nabla^C_i W_{ij} = L(r_i) \nabla_i W_{ij} \tag{21}$$

in which, $\nabla^C_i W_{ij}$ is the corrected kernel gradient; $L(r_i)$ is the renormalization matrix. For the 3D problem simulations,

$$L(r_i) = \begin{pmatrix} \sum_{j=1}^{N} x_{ji} \frac{\partial W_{ij}}{\partial x_i} \frac{m_j}{\rho_j} & \sum_{j=1}^{N} x_{ji} \frac{\partial W_{ij}}{\partial y_i} \frac{m_j}{\rho_j} & \sum_{j=1}^{N} x_{ji} \frac{\partial W_{ij}}{\partial z_i} \frac{m_j}{\rho_j} \\ \sum_{j=1}^{N} y_{ji} \frac{\partial W_{ij}}{\partial x_i} \frac{m_j}{\rho_j} & \sum_{j=1}^{N} y_{ji} \frac{\partial W_{ij}}{\partial y_i} \frac{m_j}{\rho_j} & \sum_{j=1}^{N} y_{ji} \frac{\partial W_{ij}}{\partial z_i} \frac{m_j}{\rho_j} \\ \sum_{j=1}^{N} z_{ji} \frac{\partial W_{ij}}{\partial x_i} \frac{m_j}{\rho_j} & \sum_{j=1}^{N} z_{ji} \frac{\partial W_{ij}}{\partial y_i} \frac{m_j}{\rho_j} & \sum_{j=1}^{N} z_{ji} \frac{\partial W_{ij}}{\partial z_i} \frac{m_j}{\rho_j} \end{pmatrix}^{-1} \tag{22}$$

in which, $x_{ji} = x_j - x_i$, $y_{ji} = y_j - y_i$, and $z_{ji} = z_j - z_i$.

2.8. In-house SPH code calculation procedure

The in-house SPH code can be split into three main steps (see Fig. 4). The first step involves generation of boundary particles and neighboring particles searching. The second step includes the computation of the change rates of properties to solve continuity, momentum and energy equations based on the summation of the nearest particles. The third step is to update the physical quantities at the given time step and marching these steps in an iterative manner before reaching the maximum time step. The current SPH code is based on the sample code developed by Liu and Liu [41].

ACCEPTED MANUSCRIPT

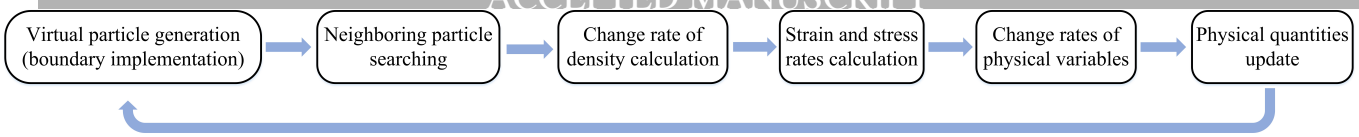

Figure 4: The calculation flowchart of the in-house SPH code.

3. Soil constitutive models

3.1. Elastoplastic constitutive model

There are several soil constitutive models, such as the Mohr-Coulomb, Drucker-Prager and Cam-Clay models to predict the soil mechanical behavior. The elastoplastic constitutive model in conjunction with the Drucker-Prager yield criterion is employed here to simulate 3D landmine detonation. The plastic deformation occurs only if the following criterion is satisfied,

$$f(I_1, J_2) = \sqrt{J_2} + \varphi_\phi I_1 - k_c \geq 0 \tag{23}$$

where $I_1 = \sigma^{\alpha\alpha}, J_2 = \frac{1}{2} S^{\alpha\beta} S^{\alpha\beta}$ are the first and the second invariants of the stress tensor, respectively. φ_ϕ and k_c are Drucker-Prager model constants which are calculated from c (cohesion) and ϕ (internal friction).

$$\varphi_\phi = \frac{\tan\phi}{\sqrt{9 + 12\tan^2\phi}} \tag{24}$$

$$k_c = \frac{3c}{\sqrt{9 + 12\tan^2\phi}} \tag{25}$$

When solving a large deformation problem, a stress rate that is invariant with respect to rigid-body rotation should be considered and incorporated into the constitutive equation. In our current research, the Jaumann stress rate $\mathring{\boldsymbol{\sigma}}$ used for the objectivity is employed as follows.

$$\mathring{\boldsymbol{\sigma}} = \dot{\boldsymbol{\sigma}} + \boldsymbol{\sigma}\dot{\boldsymbol{\omega}} - \dot{\boldsymbol{\omega}}\boldsymbol{\sigma} \tag{26}$$

in which $\dot{\boldsymbol{\sigma}}$ is the stress rate tensor. $\dot{\boldsymbol{\omega}}$ is the spin tensor defined as $\dot{\boldsymbol{\omega}} = \frac{1}{2}\left[(\nabla v) - (\nabla v)^T\right]$. The final stress-strain relationship of the soil model including plastic deformation can be derived from equations (23) and (26),

$$\frac{\mathrm{d}\sigma_i^{\alpha\beta}}{\mathrm{d}t} = \sigma_i^{\alpha\gamma}\dot{w}_i^{\beta\gamma} + \sigma_i^{\gamma\beta}\dot{w}_i^{\alpha\gamma} + 2G(\dot{\varepsilon}_i^{\alpha\beta} - \frac{1}{3}\delta_i^{\alpha\beta}\dot{\varepsilon}_i^{\gamma\gamma}) + K\dot{\varepsilon}_i^{\gamma\gamma}\delta_i^{\alpha\beta} - \dot{\lambda}_i[9K\sin\psi\delta^{\alpha\beta} + \frac{G}{\sqrt{J_2}}S_i^{\alpha\beta}] \tag{27}$$

in which, $\dot{\varepsilon}_i^{\alpha\beta}$ is the strain rate tensor; K is the elastic bulk modulus and G is the shear modulus,

$$K = \frac{E}{3(1-2\nu)} \tag{28}$$

$$G = \frac{E}{2(1+\nu)} \tag{29}$$

in which E is the young's modulus and ν is the Poisson's ratio. $\dot{\lambda}_i$ is the rate form of plastic multiplier, which is given in the following:

$$\dot{\lambda}_i = \frac{3\varphi_\phi K\dot{\varepsilon}_i^{\gamma\gamma} + (G/\sqrt{J_2})S_i^{\alpha\beta}\dot{\varepsilon}_i^{\alpha\beta}}{27\varphi_\phi K\sin\psi + G} \tag{30}$$

The particles approximations for the strain rate tensor and the spin tensor are presented as follows:

$$\dot{\varepsilon}_i^{\alpha\beta} = \frac{1}{2}\sum_{j=1}^{N}\frac{m_j}{\rho_j}(v_{ji}^\alpha\frac{\partial W_{ij}}{\partial x_i^\beta} + v_{ji}^\beta\frac{\partial W_{ij}}{\partial x_i^\alpha}) \tag{31}$$

$$\dot{w}_i^{\alpha\beta} = \frac{1}{2}\sum_{j=1}^{N}\frac{m_j}{\rho_j}(v_{ji}^{\alpha}\frac{\partial W_{ij}}{\partial x_i^{\beta}} - v_{ji}^{\beta}\frac{\partial W_{ij}}{\partial x_i^{\alpha}}) \tag{32}$$

As the elastoplastic constitutive model is implemented in this study, the soil mechanical behavior must be consistent with this model, i.e. the stress state should not be out of the yield surface when the plastic deformation occurs. However, the stress state of the soil may leave the elastic domain due to the numerical errors in computational plasticity. Therefore, the return mapping algorithm is used to return the stress state to the yield surface. According to Chen and Mizuno [42], if the stress state exceeds the apex of the yielding surface, the hydrostatic stress components should be modified based on the following equation:

$$\overline{\sigma}^{\alpha\beta} = \begin{cases} \sigma^{\alpha\beta} - \frac{1}{3}(I_1 - \frac{k_c}{\varphi_\phi})\delta^{\alpha\beta} & \text{if } -\varphi_\phi I_1 + k_c < 0 \\ \sigma^{\alpha\beta} & \text{if } -\varphi_\phi I_1 + k_c \geq 0 \end{cases} \tag{33}$$

When the stress state of the soil exceeds the yielding surface (Drucker-Prager criterion), the deviatoric shear stress components are reduced proportionally by the scaling factor R , whereas the hydrostatic component I_1 remains unchanged, according to following equations:

$$\overline{\overline{\sigma}}^{\alpha\beta} = \begin{cases} R\overline{\sigma}^{\alpha\beta} + \frac{1}{3}I_1\delta^{\alpha\beta} & \text{if } -\varphi_\phi I_1 + k_c < \sqrt{J_2} \\ \overline{\sigma}^{\alpha\beta} & \text{if } -\varphi_\phi I_1 + k_c \geq \sqrt{J_2} \end{cases} \tag{34}$$

in which $R = \frac{-\varphi_\phi I_1 + k_c}{\sqrt{J_2}}$ is a scaling factor. For more information about the soil elastoplastic model, please refer to Bui et al. [22].

It is widely reported that the SPH method suffers from instability when the material is in a state of stretching. A variety of approaches have been proposed to tackle this problems [43, 44, 45]. In this paper, the specific approach to eliminate the tensile instability is not described, as no cohesion is considered for the sand.

3.2. Hypoplastic constitutive model

In addition to the elastoplastic constitutive model, the hypoplastic model is presented as an alternative method to describe the mechanical behavior of soil. Different from the elastoplastic constitutive model, the hypoplastic model are established without the concepts of yield surface and flow rule. A general hypoplastic constitutive model was proposed by Wu and Kolymbas [46], which can be decomposed into two parts representing reversible and irreversible behaviors of soil, respectively. A rate independent hypoplastic constitutive model is considered here [46].

$$\mathring{\boldsymbol{\sigma}} = \boldsymbol{H}(\boldsymbol{\sigma}, \dot{\boldsymbol{\varepsilon}}) = \boldsymbol{L}(\boldsymbol{\sigma}) : \dot{\boldsymbol{\varepsilon}} - \boldsymbol{N}(\boldsymbol{\sigma})\|\dot{\boldsymbol{\varepsilon}}\| \tag{35}$$

in which, $\boldsymbol{L}(\boldsymbol{\sigma})$ is assumed to be linear in $\dot{\boldsymbol{\varepsilon}}$ and $\boldsymbol{N}(\boldsymbol{\sigma})$ is nonlinear in $\dot{\boldsymbol{\varepsilon}}$. $\|\dot{\boldsymbol{\varepsilon}}\| = \sqrt{tr\dot{\boldsymbol{\varepsilon}}^2}$ is an Euclidean norm.

The following specific hypoplastic constitutive model [47] is incorporated into the SPH code, which is based on a simple hypoplastic constitutive model presented by Wu and Bauer [48].

$$\mathring{\boldsymbol{\sigma}} = c_1(tr\boldsymbol{\sigma})\dot{\boldsymbol{\varepsilon}} + c_2(tr\dot{\boldsymbol{\varepsilon}})\boldsymbol{\sigma} + c_3\frac{tr(\boldsymbol{\sigma}\dot{\boldsymbol{\varepsilon}})}{tr\boldsymbol{\sigma}}\boldsymbol{\sigma} + c_4(\boldsymbol{\sigma} + \boldsymbol{\sigma}^*)\|\dot{\boldsymbol{\varepsilon}}\| \tag{36}$$

where c_1, c_2, c_3, and c_4 are dimensionless parameters; $tr()$ stands for the trace of a tensor; $\boldsymbol{\sigma}^*$ represents the deviatoric stress tensor and is defined as,

$$\boldsymbol{\sigma}^* = \boldsymbol{\sigma} - \frac{1}{3}tr(\boldsymbol{\sigma})\boldsymbol{I} \tag{37}$$

where $\boldsymbol{I}$ is the identity tensor.

ACCEPTED MANUSCRIPT

Thus, for a given particle i, the final stress-strain relationship of the hypoplastic model can be modified as,

$$\frac{d\boldsymbol{\sigma}_i}{dt} = \dot{\boldsymbol{\omega}}_i\boldsymbol{\sigma}_i - \boldsymbol{\sigma}_i\dot{\boldsymbol{\omega}}_i + c_1(tr\boldsymbol{\sigma}_i)\dot{\boldsymbol{\varepsilon}}_i + c_2(tr\dot{\boldsymbol{\varepsilon}}_i)\boldsymbol{\sigma}_i + c_3\frac{tr(\boldsymbol{\sigma}_i\dot{\boldsymbol{\varepsilon}}_i)}{tr\boldsymbol{\sigma}_i}\boldsymbol{\sigma}_i + c_4(\boldsymbol{\sigma}_i + \boldsymbol{\sigma}_i^*)\|\dot{\boldsymbol{\varepsilon}}\| \tag{38}$$

It can be observed that the stress rate tensor in equation (38) can be calculated directly from the stress tensor and strain rate tensor. The return mapping algorithm considered in the elastoplastic constitutive equation is not required in the hypoplastic model, which grately simplifies the numerical implementation in SPH.

4. Numerical validations

4.1. C4 slab explosion

The 1D C4 slab explosion is tested here to verify the explosion model in the 3D SPH code. A 0.1 m C4 slab is ignited at the left end. In order to satisify the fixed wall boundary condition, the concept of symmetrical explosive detonation is adopted, which means the detonation is initiated at the midpoint of a 0.2 m slab. As the detonation velocity of the C4 explosive charge is 8193 m/s, it takes about 12.21 μs to finish the detonation process along the C4 slab. The coeffcients of the JWL EOS for C4 explosive is shown in Table 1 [49]. The smoothing length is chosen to be $1.5\Delta x$, in which the Δx is the initial particle spacing. 2000 particles are evenly distributed in this simulation. It can be found from the Fig. 5 that the peak pressure of C4 converges to 28.5 GPa, which is in good agreement with the experimental peak pressure.

Table 1: Coefficients of the JWL model for C4.

ρ_0 (kg/m^3)	A (Pa)	B (Pa)	R_1	R_2	w	E_0 (J/kg)	v (m/s)
1601	6.098×10^{11}	1.3×10^{10}	4.5	1.4	0.25	5.621×10^6	8193

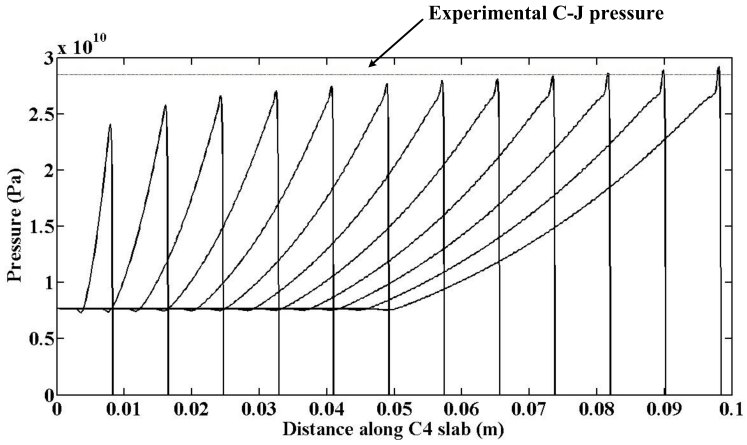

Figure 5: Pressure distribution along the 1D C4 slab during the detonation process.

ACCEPTED MANUSCRIPT

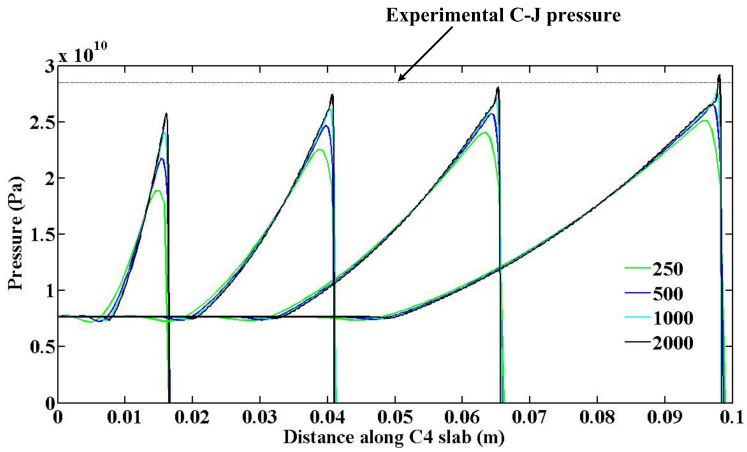

Figure 6: Pressure distribution along the 1D C4 slab with different paticles.

Furthermore, the influnce of different particle resolutions (250, 500, 1000, 2000) on the simulation results is studied. We can find from the Fig. 6 that the peak pressure increases with a growth in particle number and finally converges to 28.5 GPa, which validates the stability and reliability of the SPH method.

4.2. Sand collapse

The numerical implementations of the elastoplastic and hypoplastic models are validated by the sand collapse problem, respectively. A rectangle of sand confined between two vertical parallel plates remains static. Then the gates are opened (i.e. the plates are lifted up) and the sand is released. Thus the 3D problem can be simplified to a 2D plane strain problem solved by this 3D SPH code. The length d of this rectangle sand is 0.4 m, the height h of it is 0.1 m, and the ratio $a = h/d$ determines the collapse mode. The coefficients of elastoplastic and hypoplastic models are listed in Table 2. There are five input parameters in the constitutive models, an uncertainty analysis to quantify the influence of all uncertain input parameters on the simulation results can be conducted in the same way in research [50, 51, 52]. In this paper, the material parameters corresponds to the sand in the experiments conducted by Lube et al. [53], and are employed directly. The particle spacing is $\Delta d = 2$ mm, and 10000 particles are involved in this simulation. In addition, the non-slip boundary condition is implemented in this simulation by using three layers of dummy particles.

Table 2: The elastoplastic and hypoplastic constitutive models coefficients for the sand collapse problem [37].

	Elastoplastic constants					Hypoplastic parameters			
$\rho_0(kg/m^3)$	E (MPa)	ϕ (^{o})	ψ (^{o})	c (kPa)	ν	c_1	c_2	c_3	c_4
2100	20.0	30.0	1.0	0.0	0.25	-55.6	-171.2	-540.9	-170.9

ACCEPTED MANUSCRIPT

ACCEPTED MANUSCRIPT

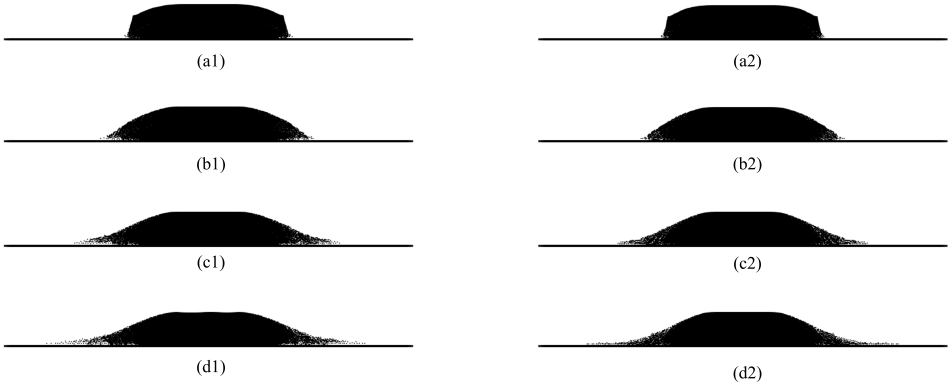

Figure 7: Collapse process of sand with the elastoplastic (a1-d1) and the hypoplastic (a2-d2) constitutive models.

The sand collapse processes using the elastoplastic and hypoplastic models are well described in Fig. 7 in terms of distribution of particles. At first, a discontinuity can be initially observed as a straight line on the upper surface of the sand column. After a while, a curve plane occurs between the static and moving particles. Finally, a parabolic-like surface profile is formed, which agrees well with the collapse process in the experiment and simulation from [53, 37].

The stresses distributions of these two models are presented in Fig. 8. It can be found that the horizontal and vertical stresses increase linearly with the depth, which is consistent with the stresses distributions of the sand confined in two parallel plates and subjected to gravity. The shear stress develops in two areas close to the wall. The reason is the sand at the bottom tend to move sideward but are restricted by the non-slip boundary condition. Therefore, these two constitutive models have been verified by the sand collapse problem.

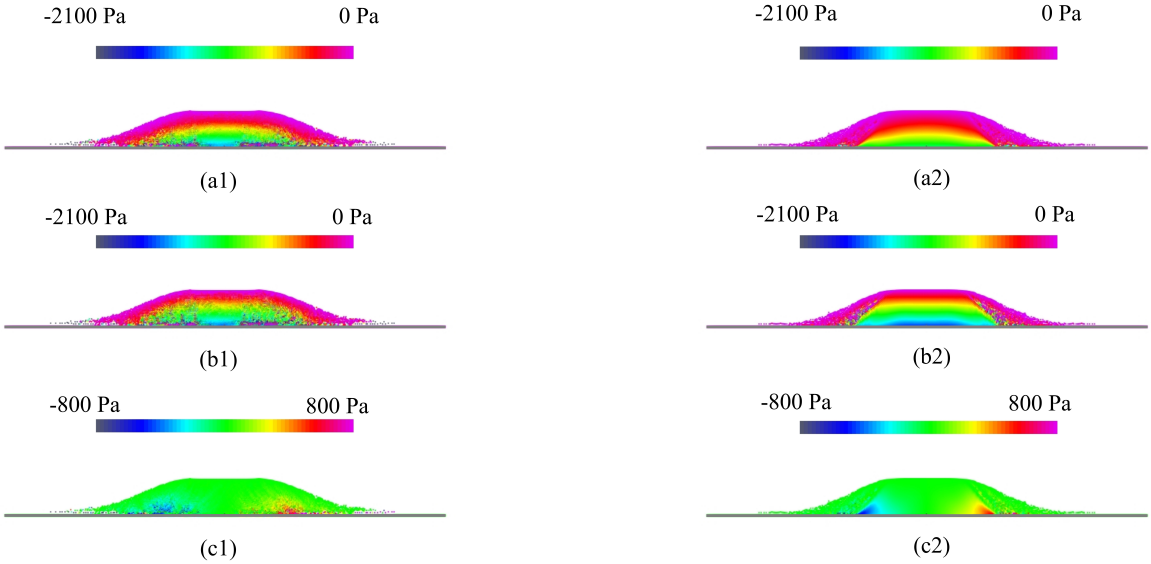

Figure 8: Stresses distributions of sand collpase problem at steady state with the elastoplastic constitutive model ((a1) horizontal stress σ_{xx}; (b1) vertical stress σ_{yy}; (c1) shear stress σ_{xy}) and the hypoplastic constitutive model ((a2) horizontal stress σ_{xx}; (b2) vertical stress σ_{yy}; (c2) shear stress σ_{xy}).

5. 3D landmine detonation

In this section, the elastoplastic and hypoplastic constitutive models are combined with the explosion model to simulate the 3D landmine detonation. The motivation of this simulation is to predict the soil ejecta generated from buried C4 explosive. The initial configuration of soil explosion simulation is shown in Fig. 9, which is exactly the same as the

ACCEPTED MANUSCRIPT

experimental geometry from [3]. A cylindrical container, with 375 mm height and 500 mm internal diameter, is filled with dry sand. A cylindrical C4 explosive charge is buried to the sand with a depth of 28 mm, and its surface is parallel to the sand surface. The coefficients of the elastoplastic and hypoplastic models used in this simulation are the same as in the sand collapse problem (see Table 2). Three layers of dummy particles are introduced to represent fixed solid boundary condition. The particle spacing is $\Delta d = 4.17$ mm, and 1,150,000 particles are involved in this simulation. The simulation time step is chosen to be $\Delta t = 1.0 \times 10^{-7}$ s. Furthermore, the Open-MP programming interface is incorporated to the in-house SPH code for the parallelization and acceleration of the computation. The CPU used here is Intel E5-2683. The total computational time for the landmine detonation is 72 CPU hours.

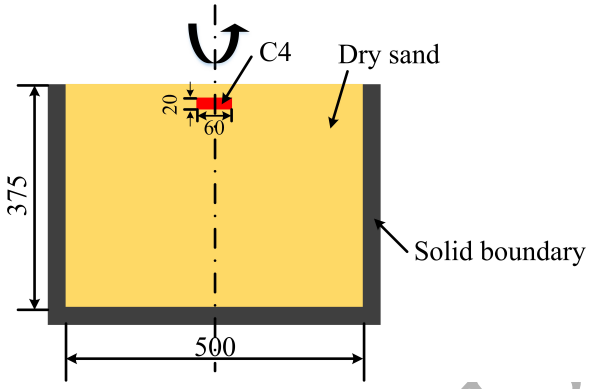

Figure 9: Initial geometry of the landmine detonation (mm).

Firstly, the elastoplastic model is used and its velocity distributions of the soil fragmentation process are shown in Fig. 10. After the ignition of the C4 explosive, a detonation wave travels outward from the detonation point. Once the shockwave reaches the edge of the explosive, most of the energy is transmitted to the surrounding soil. (see Fig. 10 (a), (b)). The particles at the top of the soil are pushed up by the detonation and gains the most momentum from the buried explosive, and a spherical dome is formed. It can be observed that the velocities of the particles at the top of the dome are always larger than the rest particles of the soil ejecta. The top soil moves much faster and this spherical dome becomes larger and larger. The profile of the soil fragmentation is like a bubble shown in Fig. 10 (d), which is close to the experimental data [3]. As the explosion gas continue to expand, the soil bubble will become thinner and rupture at some point.

ACCEPTED MANUSCRIPT

ACCEPTED MANUSCRIPT

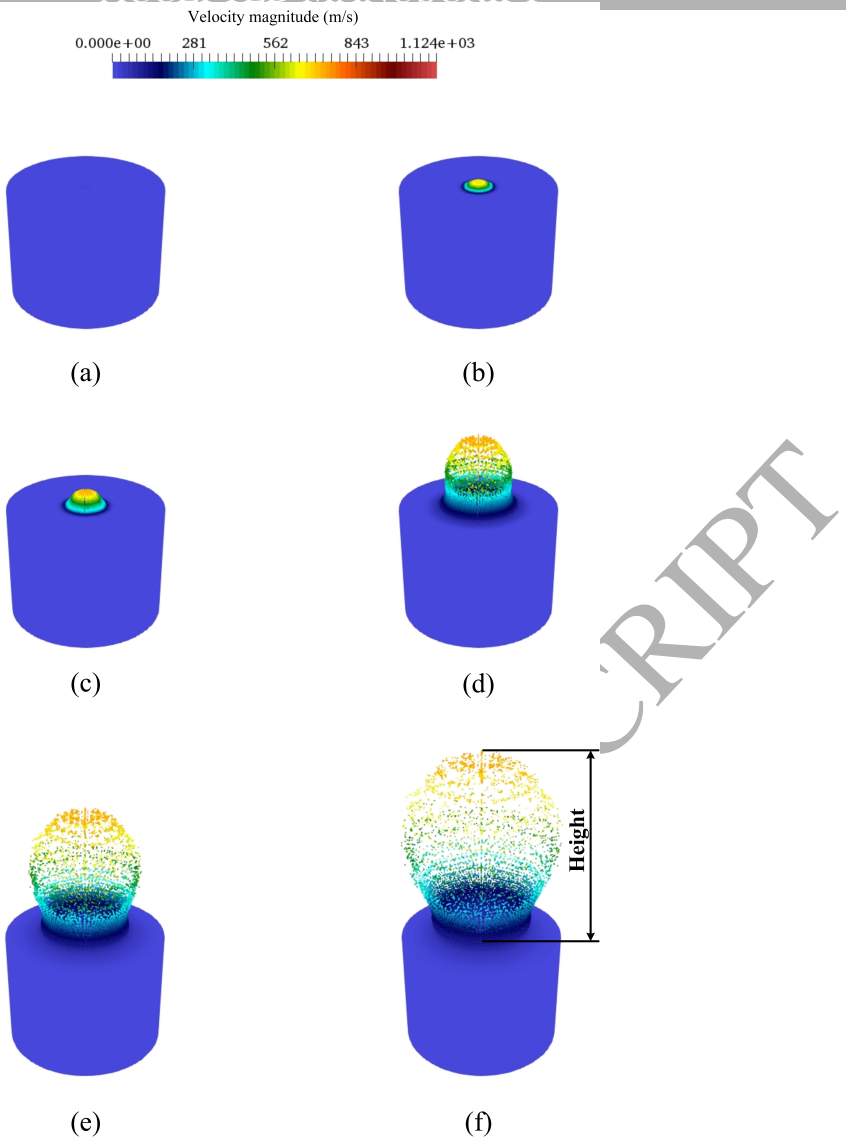

Figure 10: Velocity distributions of landmine detonation at (a) 0.01 ms; (b) 0.05 ms; (c) 0.10 ms; (d) 0.35 ms; (e) 0.60 ms; (f) 0.84 ms.

The particles density distributions are presented in Fig. 11. It shows that the densities of the soil particles below the explosive are the largest, as more resistance and compression are encountered by these particles compared to the rest of the particles surrounding the explosive charge. The detonation shock wave propagates through the interaction zone and expands the soil particles to every direction. Furthermore, the heights of load-deflection curves (see Fig. 10 (f)) for different discretizations (particle spacing of $3\Delta x$, $2\Delta x$, $1.5\Delta x$, and $\Delta x = 4.17$ mm) are investigated and shown in Fig. 12. It can be found that the heights grow with an increase in the number of particles, which converges to the values along the red line. This shows the reliablity and stability of the numerical results. Therefore, the main process of the soil fragmentation using the elastoplastic model has been captured and well described by the SPH method.

ACCEPTED MANUSCRIPT

ACCEPTED MANUSCRIPT

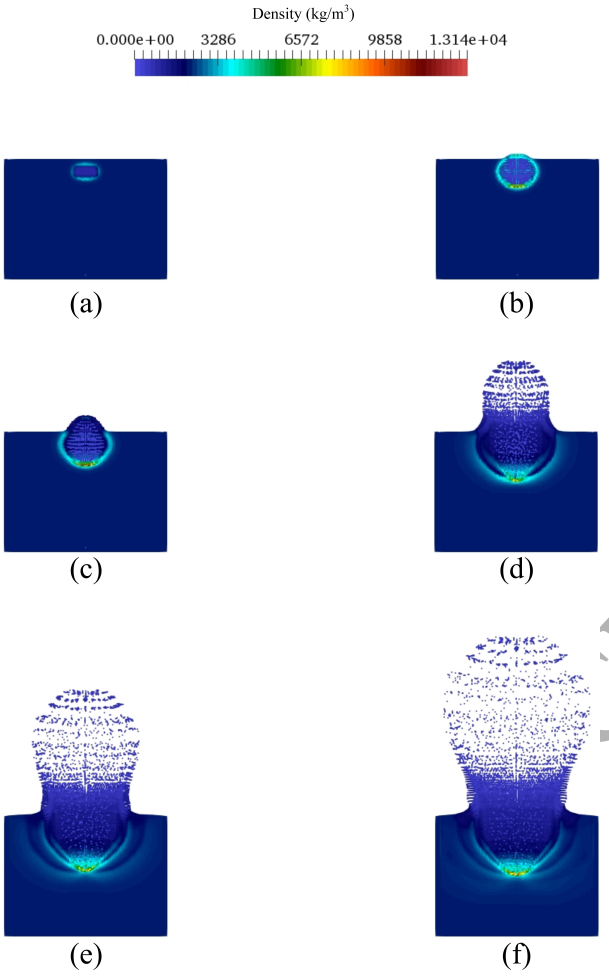

Figure 11: Density distributions of the landmine detonation at (a) 0.01 ms; (b) 0.05 ms; (c) 0.10 ms; (d) 0.35 ms; (e) 0.60 ms; (f) 0.84 ms.

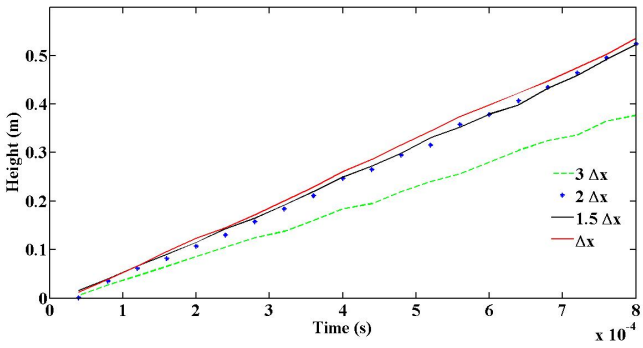

Figure 12: Height-time history of 3D landmine detonation using different discretizations.

In addition to the elastoplastic constitutive model, the hypoplastic model has also been implemented to study the detonation process. The total number of particles involved in this simulation is the same as the previous one. The velocities distributions of the landmine detonation using the hypoplastic model are presented in Fig. 13. It can be found that the soil fragmentation using this model is very similar to the soil ejecta using the elastoplastic model, and this mutual authentication strengthens the credibility of these simulation results. However, the widths obtained from the elastoplastic model are larger than those obtained from the hypoplastic model (see Fig. 14 (b4)). In order to check the validity of the 3D soil explosion model, the outline of the soil fragmentation obtained from these two constitutive models are compared with the experimental data at respective times $t = 0.03$ ms, 0.10 ms, 0.14 ms, and 0.18 ms (see Fig. 14). We can find that the

ACCEPTED MANUSCRIPT

profiles of soil ejecta at different times are very close to the experimental data. Even the extremely small soil deformation at 0.03 ms can still be captured by the SPH method (see Fig. 14 (a1, b1, c1)). Moreover, the heights and widths of the soil fragmentation are mearsured to verify the 3D landmine detonation modeling further (see Fig. 14 (b4)). Table 3 presents the heights and widths calculated from these two constitutive models, and these physical variables are very similar to the experimental measurements. The relative errors are calculated by relative error $= |sim - exp|/exp$, in which sim represents simulation results and exp denotes the experimental results. The relative error1 and error2 are calculated from the elastoplastic and hypoplastic models, respectively. It can be observed that most of the relative errors are less than 12 %, which shows that the SPH method method in conjunction with these two soil constitutive models can tackle landmine detonation problems successfully. In addition, the time history of energy balance of 3D landmine detonation using the hypoplastic constitutive model is shown in Fig. 15. It can be observed that the total energy of the landmine detonation is conserved. After the detonation of C4 explosive, the internal energy of the explosive is transferred to the kinetic energy of the sand. Thus the internal energy decreases while the kinetic energy increases rapidly. Then the sand near the expanded explosive gas interacts with the sand further, and some of the kinetic energy of the sand is converted into the internal energy of the surrounding sand. At the end, the kinetic and internal energies reach a steady state. In comparison with the results obtained from the 2D soil explosion simulations [31], the 3D soil explosion modeling yields more accurate widths and heights of the soil ejecta.

ACCEPTED MANUSCRIPT

ACCEPTED MANUSCRIPT

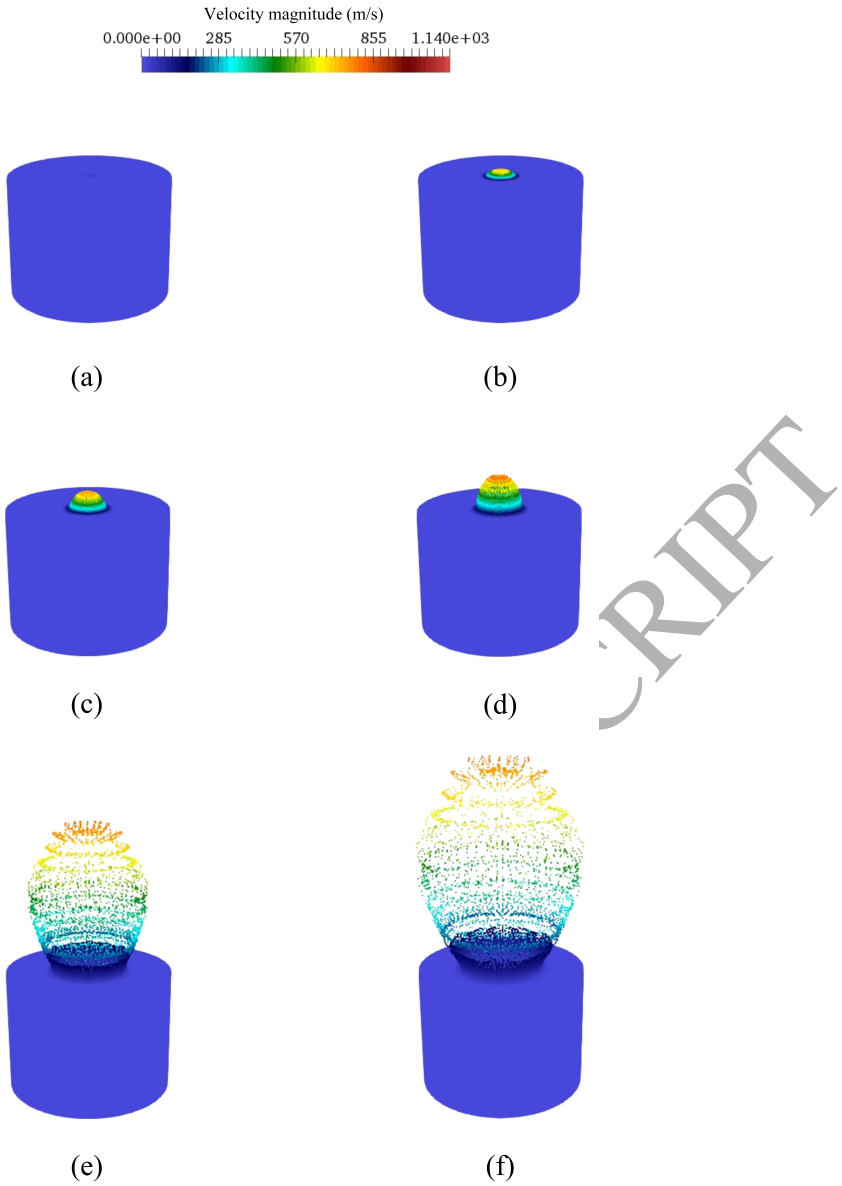

Figure 13: Velocity distributions using the hypoplastic model at (a) 0.01 ms; (b) 0.05 ms; (c) 0.10 ms; (d) 0.35 ms; (e) 0.60 ms; (f) 0.84 ms.

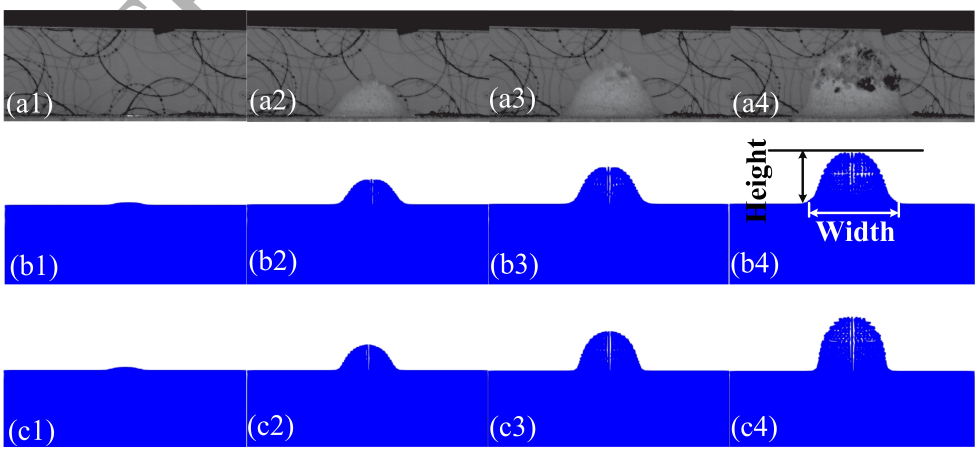

Figure 14: Comparison of the soil ejecta between the experimental [3] and simulation results, in which (a1-a4), (b1-b4) and (c1-c4) are results of the experiment, elastoplastic model, and hypoplastic model, respectively.

Table 3: Comparison of the heights and widths obtained from the experiments and simulations (mm).

	$t = 0.03$ ms		$t = 0.10$ ms		$t = 0.14$ ms		$t = 0.18$ ms	
	Height	Width	Height	Width	Height	Width	Height	Width
Experiment	5.0	33.3	55.0	120.0	82.0	136.5	115.0	180.0
Elastoplastic	5.2	37.5	52.8	130.0	76.0	160.2	98.0	200.0
Hypoplastic	5.1	37.0	52.3	109.4	75.4	132.0	97.2	160.7
Relative error1 (%)	4.0	12.6	4.0	8.3	7.3	17.2	14.7	11.1
Relative error2 (%)	2.0	11.1	4.9	8.8	8.0	3.3	15.4	11.8

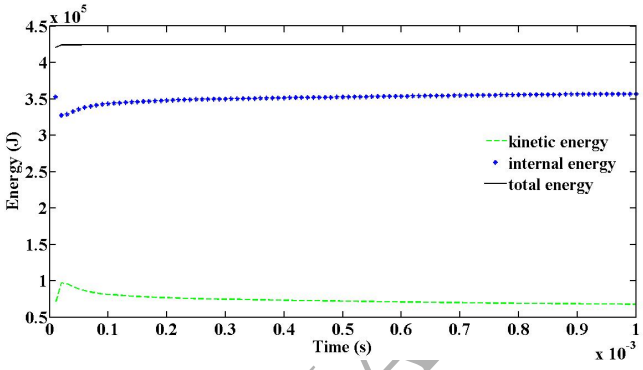

Figure 15: Time history of energy balance of 3D landmine detonation using the hypoplastic constitutive model.

6. Conclusion and future plan

The 3D landmine detonation has been a challenging task for modelling and simulation. In our current research, the modified SPH method in combination with the elastoplastic and hypoplastic constitutive models is employed to tackle the large deformation in 3D landmine detonations for the first time. The hypoplastic constitutive model, which was used to simulate the 2D granular flow problems [37], is applied for the first time to simulate the 3D soil explosion involving a large number of particles. Secondly, the original SPH cannot tackle the 3D landmine detonation directly. In order to be capable of simulating the landmine detonation problems, the original SPH method should be modified in relation to the multiphase interface treatment in our research. Thus the modified continuity equation proposed by Liu et al. for the treatment of multiphase interface in explosive welding simulation [32] is introduced to tackle the multiphase interface with large density ratio in soil explosion for the first time. In addition, the numerical results have also been compared against the fairly new experimental data conducted by Rigby et al. at the University of Sheffield [3] to validate the numerical model. As SPH is not computationally cheap, especially for the neighbouring particles searching, the Open-MP programming interface is incorporated for the parallelization and computational efficiency of the in-house SPH code. Simulation results from the elastoplastic and the hypoplastic constitutive models are compared with the experimental results, and a good agreement can be observed, which is encouraging. Several conclusions can be obtained from these simulations:

1) It has been shown that the present parallel 3D SPH method in conjunction with this modified continuity equation can handle landmine detonation problems with high density ratios very well. In addition, the widths and heights of the soil ejecta using the 3D SPH code are better predicted than our 2D SPH code.

ACCEPTED MANUSCRIPT

2) Both of the elastoplastic and hypoplastic constitutive models are appropriate for the 3D landmine detonation simulation. To our best knowledge, this is the first time these two constitutive models are implemented in SPH to investigate the landmine detonation problems.

3) More constitutive models, such as the cam-clay and the modified cam-clay constitutive models, can be implemented in the in-house SPH code to investigate the dynamic behavior of soil explosion further.

7. Acknowledgements

The authors acknowledge the group of Computational Mechanics and Design at the University of Sheffield, particularly Dr. S. E. Rigby and Prof. A. Tyas, for providing their experimental data. The first author wishes to thank the financial support from China Scholarship Council (No. 201506030072) and Natural Sciences and Engineering Research Council of Canada (NSERC). Furthermore, this work was made possible by the facilities of the Shared Hierarchical Academic Research Computing Network (SHARCNET: www.sharcnet.ca) and Compute/Calcul Canada.

References

References

[1] D. M. Bergeron, R. Walker, C. Coffey, Detonation of 100-gram anti-personnel mine surrogate charges in sand, a test case for computer code validation, National Defence, Defence Research Establishment Suffield, 1998.

[2] S. D. Clarke, S. D. Fay, J. A. Warren, A. Tyas, S. E. Rigby, J. J. Reay, R. Livesey, I. Elgy, Geotechnical causes for variations in output measured from shallow buried charges, International Journal of Impact Engineering 86 (2015) 274–283.

[3] S. E. Rigby, S. D. Fay, S. D. Clarke, A. Tyas, J. J. Reay, J. A. Warren, M. Gant, I. Elgy, Measuring spatial pressure distribution from explosives buried in dry Leighton Buzzard sand, International Journal of Impact Engineering 96 (2016) 89–104.

[4] T. Rabczuk, T. Belytschko, Cracking particles: a simplified meshfree method for arbitrary evolving cracks, International Journal for Numerical Methods in Engineering 61 (13) (2004) 2316–2343.

[5] T. Rabczuk, P. M. A. Areias, T. Belytschko, A meshfree thin shell method for non-linear dynamic fracture, International Journal for Numerical Methods in Engineering 72 (5) (2007) 524–548.

[6] T. Rabczuk, T. Belytschko, A three-dimensional large deformation meshfree method for arbitrary evolving cracks, Computer Methods in Applied Mechanics and Engineering 196 (29-30) (2007) 2777–2799.

[7] T. Rabczuk, G. Zi, S. Bordas, H. Nguyen-Xuan, A simple and robust three-dimensional cracking-particle method without enrichment, Computer Methods in Applied Mechanics and Engineering 199 (37-40) (2010) 2437–2455.

[8] T. Rabczuk, S. Bordas, G. Zi, On three-dimensional modelling of crack growth using partition of unity methods, Computers & Structures 88 (23-24) (2010) 1391–1411.

[9] T. Rabczuk, R. Gracie, J. H. Song, T. Belytschko, Immersed particle method for fluid-structure interaction, International Journal for Numerical Methods in Engineering 81 (1) (2010) 48–71.

ACCEPTED MANUSCRIPT

[10] H. L. Ren, X. Y. Zhuang, Y. C. Cai, T. Rabczuk, Dual-horizon peridynamics, International Journal for Numerical Methods in Engineering 108 (12) (2016) 1451–1476.

[11] H. L. Ren, X. Y. Zhuang, T. Rabczuk, Dual-horizon peridynamics: a stable solution to varying horizons, Computer Methods in Applied Mechanics and Engineering 318 (2017) 762–782.

[12] R. A. Gingold, J. J. Monaghan, Smoothed particle hydrodynamics: theory and application to non-spherical stars, Monthly notices of the Royal Astronomical Society 181 (3) (1977) 375–389.

[13] L. B. Lucy, A numerical approach to the testing of the fission hypothesis, The Astronomical Journal 82 (1977) 1013–1024.

[14] E. Hedayati, M. Vahedi, Numerical investigation of penetration in ceramic/aluminum targets using smoothed particle hydrodynamics method and presenting a modified analytical model, CMES-COMPUTER MODELING IN ENGINEERING & SCIENCES 113 (3) (2017) 295–323.

[15] T. Rabczuk, J. Eibl, Simulation of high velocity concrete fragmentation using SPH/MLSPH, International Journal for Numerical Methods in Engineering 56 (10) (2003) 1421–1444.

[16] T. Rabczuk, J. Eibl, Modelling dynamic failure of concrete with meshfree methods, International Journal of Impact Engineering 32 (11) (2006) 1878–1897.

[17] T. Rabczuk, J. Eibl, L. Stempniewski, Numerical analysis of high speed concrete fragmentation using a meshfree lagrangian method, Engineering fracture mechanics 71 (4-6) (2004) 547–556.

[18] D. Feng, M. Liu, H. Li, G. Liu, Smoothed particle hydrodynamics modeling of linear shaped charge with jet formation and penetration effects, Computers & Fluids 86 (2013) 77–85.

[19] G. Y. Wang, G. R. Liu, Q. Peng, S. De, D. L. Feng, M. B. Liu, A 3D smoothed particle hydrodynamics method with reactive flow model for the simulation of ANFO, Propellants, Explosives, Pyrotechnics 40 (4) (2015) 566–575.

[20] G. Y. Wang, G. R. Liu, Q. Peng, S. De, A SPH implementation with ignition and growth and afterburning models for aluminized explosives, International Journal of Computational Methods 14 (04) (2017) 1750046.

[21] X. H. Zhao, G. H. Wang, W. B. Lu, P. Yan, M. Chen, C. B. Zhou, Damage features of rc slabs subjected to air and underwater contact explosions, Ocean Engineering 147 (2018) 531–545.

[22] H. H. Bui, R. Fukagawa, K. Sako, S. Ohno, Lagrangian meshfree particles method (SPH) for large deformation and failure flows of geomaterial using elastic–plastic soil constitutive model, International Journal for Numerical and Analytical Methods in Geomechanics 32 (12) (2008) 1537–1570.

[23] H. H. Bui, K. Sako, R. Fukagawa, J. C. Wells, SPH-based numerical simulations for large deformation of geomaterial considering soil-structure interaction, in: The 12th International Conference of International Association for Computer Methods and Advances in Geomechanics (IACMAG), Vol. 1, 2008, pp. 570–578.

[24] C. Peng, W. Wu, H. S. Yu, Hypoplastic constitutive model in SPH, in: Computer methods and recent advances in geomechanics-Proceedings of the 14th International Conference of International Association for Computer Methods and Recent Advances in Geomechanics, IACMAG, 2014, pp. 1863–1868.

[25] C. Peng, X. G. Guo, W. Wu, Y. Q. Wang, Unified modelling of granular media with smoothed particle hydrodynamics, Acta Geotechnica 11 (6) (2016) 1231–1247.

ACCEPTED MANUSCRIPT

[26] X. Lai, B. Ren, H. Fan, S. Li, C. Wu, R. A. Regueiro, L. Liu, Peridynamics simulations of geomaterial fragmentation by impulse loads, International Journal for Numerical and Analytical Methods in Geomechanics 39 (12) (2015) 1304–1330.

[27] B. Ren, H. F. Fan, G. L. Bergel, R. A. Regueiro, X. Lai, S. F. Li, A peridynamics-SPH coupling approach to simulate soil fragmentation induced by shock waves, Computational Mechanics 55 (2) (2015) 287–302.

[28] H. F. Fan, G. L. Bergel, S. F. Li, A hybrid peridynamics – SPH simulation of soil fragmentation by blast loads of buried explosive, International Journal of Impact Engineering 87 (2016) 14–27.

[29] H. F. Fan, S. F. Li, A peridynamics-SPH modeling and simulation of blast fragmentation of soil under buried explosive loads, Computer Methods in Applied Mechanics and Engineering 318 (2017) 349–381.

[30] H. Fan, S. Li, Parallel peridynamics-SPH simulation of explosion induced soil fragmentation by using OpenMP, Computational Particle Mechanics 4 (2) (2017) 199–211.

[31] J. Y. Chen, F. S. Lien, Simulations for soil explosion and its effects on structures using SPH method, International Journal of Impact Engineering 112 (2018) 41–51.

[32] M. B. Liu, Z. L. Zhang, D. L. Feng, A density-adaptive SPH method with kernel gradient correction for modeling explosive welding, Computational Mechanics.

[33] J. J. Monaghan, An introduction to SPH, Computer Physics Communications 48 (1) (1988) 89–96.

[34] J. J. Monaghan, Simulating free surface flows with SPH, Journal of Computational Physics 110 (2) (1994) 399–406.

[35] L. D. Libersky, A. G. Petschek, T. C. Carney, J. R. Hipp, F. A. Allahdadi, High strain lagrangian hydrodynamics: a three-dimensional SPH code for dynamic material response, Journal of Computational Physics 109 (1) (1993) 67–75.

[36] S. Adami, X. Y. Hu, N. A. Adams, A generalized wall boundary condition for smoothed particle hydrodynamics, Journal of Computational Physics 231 (21) (2012) 7057–7075.

[37] C. Peng, W. Wu, H. S. Yu, C. Wang, A SPH approach for large deformation analysis with hypoplastic constitutive model, Acta Geotechnica 10 (6) (2015) 703–717.

[38] W. K. Liu, S. Jun, Y. F. Zhang, Reproducing kernel particle methods, International Journal for Numerical Methods in Fluids 20 (8-9) (1995) 1081–1106.

[39] J. Shao, H. Li, G. Liu, M. Liu, An improved SPH method for modeling liquid sloshing dynamics, Computers & Structures 100 (2012) 18–26.

[40] G. Oger, M. Doring, B. Alessandrini, P. Ferrant, An improved SPH method: Towards higher order convergence, Journal of Computational Physics 225 (2) (2007) 1472–1492.

[41] G. R. Liu, M. B. Liu, Smoothed particle hydrodynamics: a meshfree particle method, World Scientific, 2003.

[42] W. F. Chen, E. Mizuno, Nonlinear analysis in soil mechanics, Elsevier Amsterdam, 1990.

[43] J. Gray, J. Monaghan, R. Swift, SPH elastic dynamics, Computer Methods in Applied Mechanics and Engineering 190 (49) (2001) 6641–6662.

[44] T. Rabczuk, T. Belytschko, S. Xiao, Stable particle methods based on lagrangian kernels, Computer Methods in Applied Mechanics and Engineering 193 (12) (2004) 1035–1063.

ACCEPTED MANUSCRIPT

[45] C. Zhang, X. Y. Hu, N. A. Adams, A generalized transport-velocity formulation for smoothed particle hydrodynamics, Journal of Computational Physics 337 (2017) 216–232.

[46] W. Wu, D. Kolymbas, Numerical testing of the stability criterion for hypoplastic constitutive equations, Mechanics of Materials 9 (3) (1990) 245–253.

[47] X. T. Wang, W. Wu, An updated hypoplastic constitutive model, its implementation and application, in: Bifurcations, Instabilities and Degradations in Geomaterials, Springer, 2011, pp. 133–143.

[48] W. Wu, E. Bauer, A simple hypoplastic constitutive model for sand, International Journal for Numerical and Analytical Methods in Geomechanics 18 (12) (1994) 833–862.

[49] D. Dooge, R. Dwarampudi, G. Schaffner, A. Miller, R. T, M. Vunnam, V. Babu, Evolution of occupant survivability simulation framework using FEM-SPH coupling, Tech. rep. (2011).

[50] T. Vu-Bac, N L, X. Y. Zhuang, T. Nguyen-Thoi, T. Rabczuk, A software framework for probabilistic sensitivity analysis for computationally expensive models, Advances in Engineering Software 100 (2016) 19–31.

[51] K. M. Hamdia, M. Silani, X. Y. Zhuang, P. F. He, T. Rabczuk, Stochastic analysis of the fracture toughness of polymeric nanoparticle composites using polynomial chaos expansions, International Journal of Fracture 206 (2) (2017) 215–227.

[52] K. M. Hamdia, H. Ghasemi, X. Y. Zhuang, N. Alajlan, T. Rabczuk, Sensitivity and uncertainty analysis for flexoelectric nanostructures, Computer Methods in Applied Mechanics and Engineering 337 (2018) 95–109.

[53] G. Lube, H. E. Huppert, R. S. J. Sparks, A. Freundt, Collapses of two-dimensional granular columns, Physical Review E 72 (4) (2005) 041301.

ACCEPTED MANUSCRIPT